Journal of Materials Chemistry C

Accepted Manuscript

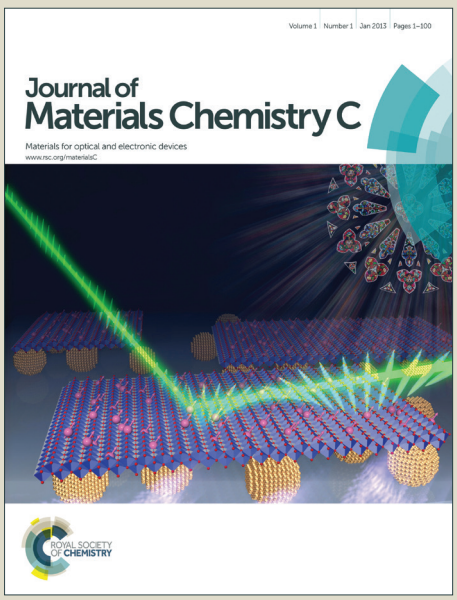

ROYAL SOCIETY OF CHEMISTRY

www.rsc.org/materialsC

Electronic and Transport Properties of Porous Graphene Sheets and Nanoribbons: Benzo-CMPs and BN codoped Derivatives

Si Li, [a] Zhao-Di Yang,*[a] Guiling Zhang [a] and Xiao Cheng Zeng*[b]

[a]*College of Chemical and Environmental Engineering, Harbin University of Science and Technology, Harbin 150040, China*

[b]*Department of Chemistry, University of Nebraska-Lincoln, Lincoln, Nebraska, 68588, USA.*

*E-mail: yangzhaodi@163.com; xzeng1@unl.edu

†Electronic supplementary information (ESI) available: Schematic diagram of method shearing two dimensional porous graphene sheet into different kind of nanoribbons; PDOS of two-probe device of 3-Benzo-CMP, BN-3-Benzo-CMP and BN-p-3ZGNR(w=4) at 0.0 and 2.0 V bias voltage; I–V_b curves of BN-p-3AGNR(w=2), BN-p-4AGNR(w=2), BN-p-5AGNR(w=2), BN-p-4ZGNR(w=4) and BN-p-5ZGNR(w=4).

Abstract We investigate the electronic and electron transport properties of a series of 2D porous *n*-Benzo-CMPs (CMP refers to π-conjugated microporous polymers) sheets with different pore size *n* and their boron-nitride (BN) codoped derivatives, BN-*n*-Benzo-CMPs, as well as one-dimensional (1D) porous graphene nanoribbons (p-GNRs) tailored from *n*-Benzo-CMPs and BN-*n*-Benzo-CMPs using density-functional theory (DFT) and the non-equilibrium Green's function (NEGF) methods. We find that the *n*-Benzo-CMPs and BN-*n*-Benzo-CMPs (n = 3, 4, 5) sheets are all semiconductors with direct band gaps (0.57 - 1.75 eV). Their band gap decreases with increasing the pore size *n*. In addition, the 1D armchair and zigzag P-GNRs tailored from 2D *n*-Benzo-CMPs and BN-*n*-Benzo-CMPs (n = 3, 4, 5) sheets are all semiconductor with the band gaps ranging from 0.19 to 2.0 eV. BN codoping, pore size (n), and the width of nanoribbons (w) can all be used to tune the band gap of either 2D porous graphenes or their corresponding 1D p-GNRs. Computed current–voltage (I–V_b) curves are consistent with the semiconducting properties and suggest that both BN-3-Benzo-CMP and BN-p-3ZGNR (w = 4) can be exploited for applications in low-dimensional electronics.

1. Introduction

Graphene, a two-dimensional (2D) atomic layer material, is known to possess many unusual properties, such as high carrier mobility, long spin relaxation time, linear dispersion relation, quantum tunneling effect, and half integer quantum hall effect at room temperature[1-5]. However, the perfect graphene sheet exhibits zero bandgap, a limitation that must be overcome for its wide applications in nanoelectronics. Several approaches have been introduced to open up a band gap for graphene, including doping (transition metal-doping or BN-doping), grafting with functional groups, or making graphene nanoribbons directly. Another scalable approach to open the band gap is through the synthesis of porous graphene. Porous graphene refers to as graphene-like structures with nanometer-scale pores. Bieri *et al*. have successfully synthesized 2D polyphenylene,[6] a prototype of porous graphene whose direct band gap is in the range of 2.3–3.2 eV.[7-10] Later, some other porous graphene-like structures, namely, biphenylene carbon (BPC) nanosheet and its BN derivatives, are designed and studied theoretically.[11,12] The CMPs are a class of porous frameworks consisting of an extended π-conjugated network and inherent nanopores. A 2D sheet of the CMPs can be categorized as "porous graphenes".[13] Jiang *et al.* synthesized porous frameworks based on aza-fused CMPs with pore size of 1.4 nm. This new 2D material possesses novel functions for potential applications as super-capacitor in energy storage or in electric power supply.[14] Inspired by the successful synthesis of aza-fused CMP, we previously investigated electronic and electron transport properties of the 2D benzo-CMP and aza-CMP sheets and their BN codoped derivatives using DFT calculations and the non-equilibrium Green's function (NEGF) method.[15] The computation results show that both benzo-CMP and aza-CMP are semiconductors with direct band gap of 0.92 and 1.07 eV, respectively. The BN codoped derivatives possess narrower band gaps (0.47 - 0.60 eV). The tunable electronic and electron transport properties *via* BN codoping of benzo-CMP or aza-CMP can be exploited for applications in low-dimensional electronics. In this study, our focus is mainly placed on three new 2D porous graphene structures constructed by replacing each double bond in the graphene with either three, four, or five fused benzenes (denoted as *n*-Benzo-CMP, *n* = 3, 4, 5). A particular aim is to investigate effect of pore size *n* on the electronic and transport properties. Properties of the corresponding BN codoped derivatives (denoted as BN-*n*-Benzo-CMPs, *n* = 3, 4, 5) are also studied.

Graphene can be tailored into quasi one-dimensional (1D) graphene nanoribbons (GNRs) along

different rolling-up vector directions. Two prototype GNRs which have been extensively studied are the armchair- and zigzag-edged GNRs (AGNRs and ZGNRs). Considerable research effort has been made to modify the properties of GNRs, such as the effect of width,[16, 17] defects,[18] doping,[19] adsorption,[18, 20] shape (F-terminated helical,[21] tri-wing[22]) or edges[23, 24] on the electronic and magnetic properties of GNRs. In this study, we also investigate electronic and transport properties of 1D nanoribbons of porous graphene and the corresponding BN codoped derivatives.

2. Computational details

Geometry optimizations and electronic structure calculations for the periodic systems are based on density functional theory (DFT) methods implemented in the SIESTA package.[25] The generalized gradient approximation (GGA) in the Perdue-Burke- Ernzerhof (PBE) form is used to treat the exchange-correlation potential[26] and the double-ζ polarization (DZP) basis sets are selected for the DFT calculations. A real-space grid with an equivalent energy cutoff of 150 Ry is adopted to expand the electron density for numerical integration. A vacuum layer greater than 10 Å is used to avoid interaction among periodic images. All the atoms in the unit cell are fully relaxed with the force on each atom being less than 0.01 eV/Å and the total energy changes being less than 0.0001 eV. The Brillouin zone is sampled at 1×50×50 (*x*, *y*, *z* directions, respectively) Monkhorst meshes for 2D structures and 1×1×100 Monkhorst meshes for 1D structures.

The computations for the two-probe systems are performed using an *ab initio* computation software package, Atomistix ToolKit (ATK),[27] which is based on a combination of DFT and the non-equilibrium Green's function (NEGF) methods. In the computation system, the left and right electrodes are chosen to be the half of the scattering region. Transport current is computed by changing the applied bias in the step of 0.2 V and in the range of 0.0 to 2.0 V. The current through the system is computed according to the Landauer–Büttiker formula[28]

$$I = G_0 \int T(E, V_b)[f_L(E) - f_R(E)]dE$$

where $G_0 = 2e^2 / h$ is the unit of quantum conductance, $T(E, V_b)$ is the transmission coefficient at energy E and the bias voltage V_b, and $f_{R(L)}(E)$ are the Fermi distribution functions at right (left)

electrode. For the two-probe systems, GGA/PBE is also employed to describe the exchange correlations between electrons while DZP basis sets are used for all atoms.

3. Results and Discussions

3.1 Geometrical structures and electronic properties of 2D porous CMP sheets

The optimized structures of 2D porous CMPs, *n*-Benzo-CMPs (*n* = 3, 4, 5) and BN-*n*-Benzo-CMPs (*n* = 3, 4, 5), are shown in Fig. 1. The lattice parameters (*b*=*c*) and computed band gaps for these 2D structures are collected in Table 1. Here, the 2D *n*-Benzo-CMPs (*n* = 3, 4, 5) are initially constructed by replacing each double bond in graphene with either three, four or five fused-benzenes to exhibit planar graphene-like honeycomb structures (see Fig. 1(a, c, e)). The optimized lattice constants are 8.64, 12.90, and 17.27 Å, and the pore diameters are 3.68, 8.25, and 12.22 Å, for 3-Benzo-CMP, 4-Benzo-CMP, and 5-Benzo-CMP, respectively. As shown in Fig. 1(a, c, e), there are two different carbon sites in *n*-Benzo-CMPs, labeled C_1 and C_2. C_1 atoms are bonded with three carbon atoms while C_2 atoms are bonded with two carbon and one hydrogen atoms. The average bond length of C_1-C_1 (1.46 Å) is longer than that of C_1-C_2 (1.40 Å). The BN codoped derivatives BN-*n*-Benzo-CMPs (*n* = 3, 4, 5) are initially constructed by replacing C_1 hexagonal rings in the primitive unit cell of *n*-Benzo-CMPs with hexagonal BN rings. Our previous study indicates that two hexagonal BN rings in the primitive unit cell prefer a *trans*-position arrangement.[15] Hereafter, we focus mainly on the *trans*-position arrangement for BN-*n*-Benzo-CMPs (*n* = 3, 4, 5) (Fig. 1(b, d, f)). The optimized lattice constants of BN-*n*-Benzo-CMPs are 8.83, 13.08, and 17.36 Å for *n* =3, 4, and 5, respectively, all slightly longer than those of the *n*-Benzo-CMPs. The pores of BN-*n*-Benzo-CMPs deform slightly and their average diameters are approximately 3.84, 8.40, and 12.93 Å for *n* =3, 4, and 5, respectively, again slightly larger than those of undoped *n*-Benzo-CMPs. This is because the B-N bond (1.49 Å) is longer than the C_1-C_1 bond (1.46 Å), leading to slightly larger hexagonal BN rings, thereby larger lattice constants and pore sizes than the *n*-Benzo-CMPs counterparts. The deformation of the pores in B*N*-*n*-Benzo-CMPs mainly arises from the uneven bond lengths of B-C_2 (1.50 Å) and *N*-C_2 (1.37 Å).

Next, we show computed electronic properties of *n*-Benzo-CMPs and BN-*n*-Benzo-CMPs (*n* = 3, 4, 5). The electronic band structures are plotted in Fig. 2, together with the density of states (DOS). Clearly, all *n*-Benzo-CMPs are semiconductors with direct band gap at the Γ point. The band gaps of *n*-Benzo-CMPs are 1.75, 1.52, and 0.92 eV for *n* = 3, 4, and 5, respectively, all less than that of polyphenylene network (~2.35 eV).[7-10] Notably the band gap decreases with increasing the pore size *n*. In other words, larger pore size results in smaller band gap. From the partial density of states (PDOS) of *n*-Benzo-CMPs (right panel of Fig. 2(a, c, e)), one can see that both C_1 and C_2 atoms contribute to the valence band maximum (VBM) and the conduction band minimum (CBM). With increasing *n*, the contribution from C_2 atoms increases gradually, while that from C_1 atoms decreases. For *n* = 5, the contribution from C_2 is obviously more pronounced than that from C_1. Hence, the C_2 contribution plays an important role in lowering the band gap. The wave functions corresponding to the VBM and CBM states are plotted in the insets of Fig. 2(a, c, e). The VBM of 3-Benzo-CMP stems mainly from the π orbitals of C_1–C_2 and C_1–C_1 bonds, and the CBM is dominated by the p_z orbitals of C_2 atoms and the antibonding π orbitals of C_1–C_2 and C_1–C_1 bonds. From the wave functions of 4-Benzo-CMP shown in Fig. 2(c), the VBM stems mainly from the π orbitals of C_1–C_2 bonds, while the CBM mainly from the π orbitals of C_1 hexagonal rings and the p_z orbitals of C_2 atoms. In Fig. 2(e), the wave functions of 5-Benzo-CMP show that the VBM of 5-Benzo-CMP is mainly contributed by the p_z orbitals of C_2 atoms and the π orbitals of C_1–C_2 bonds, and the CBM is mainly contributed by the π orbitals of C_1 hexagonal rings and the p_z orbitals of C_2 atoms. With increasing *n*, the contribution from p_z orbitals of C_2 gradually increases, demonstrating again the effect of C_2 on lowering the band gap.

In addition, the electronic band structures of BN codoped derivatives, B*N*-*n*-Benzo-CMPs (*n* = 3, 4, 5), are given in Fig. 2(b, d, f). All BN codoped derivatives display semiconducting features with direct band gap of 1.19, 0.90, and 0.57 eV for *n* = 3, 4, and 5, respectively. Again, the band gap decreases with increasing the pore size *n*. Compared with *n*-Benzo-CMP counterparts, BN codoped derivatives possess narrower band gap. Obviously, the BN codoping plays an important role in changing the band gap. In our previous work, the effect of BN codoping on lowering the band gap was discussed in detail through analyzing the PDOS of B and N atoms and the wavefunctions of the VBM and CBM at Γ point.[15] Here, the same analysis is applied to the *n*-Benzo-CMPs.

3.2 Geometrical structures and electronic properties of porous graphene nanoribbons

1D armchair- and zigzag-edged p-GNRs (p-AGNRs and p-ZGNRs) can be viewed as tailoring a rectangle piece from graphene along different direction (see ESI Fig. S1†). Like AGNRs and ZGNRs, p-AGNRs and p-ZGNRs can be also defined on the basis of the number of dimer lines (denoted as N_a) and the number of zigzag chains (denoted as N_z). First, regardless of the pore size (using n = for 3 as an example), the three p-AGNRs and three p-ZGNRs tailored form 3-Benzo-CMP are named as p-3AGNR ($w = N_a$) and p-3ZGNRs ($w = 2N_z$), respectively (see Fig. 3(a-c) and Fig. 4(a-c)). Here the width parameter N_a is set as 3, 4, and 5, respectively, while the N_z is chosen to be 2, 3, and 4 so that the effect of the width of p-GNRs on the electronic properties can be investigated. For comparison, BN-p-3AGNR (w = 3, 4, 5) and BN-p-3ZGNRs (w = 4, 6, 8) are derived from BN-3-Benzo-CMP so that effects of BN codoping and the width on the band gap of 1D BN-p-GNRs can be investigated (see Fig. 3(d-f)) and Fig. 4(d-f)). Among all the armchair- and zigzag-edged p-GNRs considered (see Figs. 3 and 4), the BN-p-3ZGNR (w=4) exhibits smaller band gap and better electron transport property. Besides, BN-p-4ZGNR (w=4), BN-p-5ZGNR (w=4), and BN-p-nAGNR (w=2, n=3, 4, 5) derived from BN-n-Benzo-CMP (n= 3, 4, 5) are also investigated. The latter are the narrowest BN-codoped p-AGNRs with different n (Fig. 5).

For all p-GNRs, the geometrical optimizations and electronic properties are computed using the same methods implemented in Siesta package. The data of lattice parameters and band gaps are summarized in Table 2. The lattice constants of p-3AGNRs (w = 3, 4, 5) are 14.97Å, and those of p-3ZGNRs (w = 4, 6, 8) are 8.64 Å. All p-3AGNRs and p-3ZGNRs possess the same nanometer-scale pores. The lattice constants of BN-p-3AGNRs (w = 3, 4, 5) and BN-p-3ZGNRs (w=4, 6, 8) are 15.30 and 8.84 Å, respectively, slightly larger than those of p-3AGNRs and p-3ZGNRs. With increasing the pore size, the lattice constants are in the order of BN-p-3ZGNRs (8.84 Å) < BN-p-4ZGNR (w = 4) (13.08 Å) < BN-p-5ZGNR (w = 4) (17.37 Å). Unlike other pore-containing nanoribbons, the three BN-p-nAGNRs (w = 2, n = 3, 4, 5) exhibit ladder-shaped structure (Fig. 5) and the lattice constants of BN-p-3AGNRs (w = 2), BN-p-4AGNRs (w = 2) and BN-p-5AGNRs (w = 2) are 15.29, 22.67, and 30.06 Å, respectively.

Computed band structures and PDOS of p-3AGNRs (w=3, 4, 5) and p-3ZGNRs (w=4, 6, 8) are shown in Fig. 6. Clearly, both armchair and zigzag p-GNRs are semiconductors with direct band gap at Γ point. The band gaps of p-3AGNRs (w=3, 4, 5) are 2.00, 1.94, and 1.92 eV, respectively, and

those of p-3ZGNRs (w = 4, 6, 8) are 1.91, 1.87, and 1.84 eV, respectively, all larger than that of 2D 3-Benzo-CMP sheet (1.75 eV). With increasing of the width, the band gaps of p-3AGNRs and p-3ZGNRs decrease slightly. These results can be attributed to the more extended π conjugation in the wider nanoribbons. The PDOS and wave functions at the Γ point of VBM and CBM do not show significant changes even with the 3-Benzo-CMP being tailored into nanoribbons (c.f. Fig. 6).

The band structures and PDOS of BN-codoped p-GNRs are shown in Fig. 7. Here, all BN-p-3AGNRs (w = 3, 4, 5) and BN-p-3ZGNRs (w = 4, 6, 8) are semiconductors with direct band gap at Γ point. The band gaps of armchair BN-p-3AGNRs are 1.27, 1.08, and 1.21 eV for w=3, 4, and 5, and those of zigzag BN-p-3ZGNRs are 1.14, 1.15, and 1.16 eV for w=4, 6, 8, respectively (see Table 2). These values are uniformly smaller than those of hydrocarbon p-GNR counterparts, indicating that the BN codoping in 1D p-GNRs tends to reduce the band gap, as in the case of 2D porous graphene. For zigzag BN-p-3ZGNRs, their band gaps show little change with increasing the width from 4-8 and are very close to the corresponding 2D (B*N*-3-Benzo-CMP) analogues (1.19 eV). This is because the structures of BN-p-3ZGNRs are similar to those of 2D analogues except the hydrogen passivation (see Fig. 4). For BN-p-3AGNRs (w =2, 3, 4, 5), as shown in Table 2, Fig. 7 and Fig. 9, there is no regular trend in band gap changes with increasing the width. For w = 3 and 5, the band gaps of BN-p-3AGNRs are larger than that of the BN-3-Benzo-CMP sheet (1.19 eV). However, for w = 2 and 4, the band gaps of BN-p-3AGNRs are smaller than that of BN-3-Benzo-CMP sheet. From the wavefunctions shown in Fig. 7(b) and Fig. 9(a), one can see that the VBM and CBM of BN-p-3AGNRs correspond to all intramolecular charge transfer states, thereby giving smaller band gaps than those without BN codoping. Therefore, BN codoping is a useful means to reduce the band gap. Meanwhile, the width of nanoribbons can be also used to adjust the band gap of 2D porous graphenes.

To investigate the effect of pore size n on the electronic structure of 1D BN codoped p-GNRs, we select the narrowest zigzag BN-p-nZGNR (w = 4, n = 3, 4, 5) and armchair BN-p-nAGNR (w = 2, n = 3, 4, 5) as examples to compute the band structures and PDOS (see Figs. 8, and 9). For BN-p-nZGNR (w = 4, n = 3, 4, 5), the band gaps are in order of n = 3 (1.14 eV) > n = 4 (0.83 eV) > n = 5 (0.52 eV), suggesting that enlarging pore size results in smaller band gap. This trend is in line with the conclusion of 2D porous CMP sheets. For ladder-shaped BN-p-nAGNR (w = 2, n = 3, 4, 5), the band gaps are 0.93, 0.38, and 0.19 eV for BN-p-3AGNR (w=2), BN-p-4AGNR (w=2),

BN-p-5AGNR (w=2), respectively, again following the order of $n = 3 > n = 4 > n = 5$. Therefore, regardless of chirality of 1D BN codoped p-GNRs, the band gaps always decrease with increasing of pore size n.

On the basis of discussions above, BN-codoping appears to be an effective approach to reduce the band gap for either 2D porous graphenes or 1D p-GNRs. Moreover, the band gaps decrease with enlarging the pore size, regardless of dimensionality, chirality of nanoribbons and B**N**-codoping. Lastly, the width is another design parameter that can either enlarge or reduce the band gap of 1D p-GNRs or BN-p-GNRs. Note also that the GGA functional tends to underestimate the band gap of semiconductors. As an example, for the porous graphene formed by 2D polyphenylene, the GGA functional predicts the band gap to be about 2.3-2.5 eV.[7,9,10] Du and coworkers also computed the band gap of 2D polyphenylene using the more accurate hybrid HSE06 functional and predicted the band gap to be about 3.2 eV. Comparing the band structures based on the GGA and HSE06 functionals, one can see that both valence bands have similar dispersions, but the conduction band minimum computed with the HSE06 shifts to higher energy with respect to the Fermi level. Nevertheless, other than the value of band gap, the predicted electronic structures of porous graphenes from either the GGA or the HSE06 functional are qualitatively the same.

3.3 Transport properties of two-probe devices

In addition to the electronic structures, we also compute the electron transport properties and I–V_b characteristics of 3-Benzo-CMP and BN-3-Benzo-CMP sheets. The two-probe system employed for 3-Benzo-CMP sheets is shown in Fig. 10(a), in which the 3-Benzo-CMP is taken as an example to show the composition of two-probe system. As shown in Fig. 10(a), both electrodes and the central region are made of the 2D 3-Benzo-CMP sheet. (Note that the electrodes considered here are semiconductors, and the semiconducting electrodes have been previously considered by several groups.[29-31]) The transmission is set in the z direction. Periodic boundary conditions are imposed in the y directions (normal the z direction). The I–V_b curves for 3-Benzo-CMP and B*N*-3-Benzo-CMP sheets are shown in Fig. 10(b). The computed zero-bias transmission spectra for 3-Benzo-CMP and BN-3-Benzo-CMP sheets are shown in Fig. 10(c), together with the transmission spectra at 2.0 V bias voltages.

For the two-probe system of the 3-Benzo-CMP sheet, a region of zero transmission with width of 1.60 eV is located around the Fermi level (see Fig. 10(c)), coinciding with the computed band gap (1.75 eV) of 3-Benzo-CMP sheet. The I–V_b curve of the 3-Benzo-CMP sheet exhibits typical semiconducting behavior with weak current response. The system possesses a threshold voltage V_{th}= 1.8 V below which the current is nearly zero. When the bias voltage increases to 2.0 V, the current is merely 0.2 μA. This current is mainly attributed to the transmission coefficient around the Fermi level within the bias window. For the transmission spectra at 2.0 V bias voltage (Fig. 10(c)), a low transmission coefficient peak is seen around the Fermi level within the bias window [-1.0 V, 1.0V]. The PDOS of the two-probe system at 0.0 and 2.0 V bias voltage is also consistent with the conclusion shown in ESI Fig. S2.

For the two-probe system of BN-3-Benzo-CMP sheet, the width of zero transmission is 1.16 eV (see Fig. 10(c)), in good agreement with the computed band gap (1.19 eV) of BN-3-Benzo-CMP. The I–V_b curve of BN-3-Benzo-CMP also exhibits typical semiconducting behavior. However the threshold voltage (V_{th} = 1.4 V) is less than that of the 3-Benzo-CMP sheet, consistent with the computed electronic properties. Namely, the BN codoping can reduce the band gap of porous graphene. When the bias voltage is increased, the current increases up to 3.64 μA under 2.0 V. The transmission spectra at 2.0 V bias voltage show that there is a relatively strong transmission peak around the Fermi level within the bias window [-1.0 V, 1.0 V]. So the BN codoping of 3-Benzo-CMP sheet can enhance the conductivity, thereby more suitable for applications in molecular electronics.

Among all 1D p-GNRs and their BN codoped derivatives discussed in Sec. 3.2, BN-p-nZGNR (w = 4, n = 3, 4, 5) and BN-p-nAGNR (w = 2, n = 3, 4, 5) are chosen for computing their I–V_b curves because these systems exhibit relatively narrow band gaps. However, most of these systems show small current response (a few nA). The I–V_b curves of BN-p-3AGNR (w = 2), BN-p-4AGNR (w = 2), BN-p-5AGNR (w = 2), BN-p-4ZGNR (w = 4) and BN-p-5ZGNR (w = 4) are presented in ESI Fig. S3. Only BN-p-3ZGNR (w = 4) gives relatively strong current response. Thus, only the electron transport property of this BN codoped p-ZGNRs is further discussed. Schematic view of the two-probe system of BN-p-3ZGNR (w = 4) is plotted in Fig. 11(a). Here, the transmission is in the z direction as well but no periodic boundary conditions are imposed in the y direction. The I–V_b curve of BN-p-3ZGNR (w = 4) is given in Fig. 11(b), showing typical semiconducting behavior. The

threshold voltage is 1.2 V below which the current is nearly zero. Beyond 1.2 V the current increases with increasing the bias voltage. At 2.0 V bias voltage the current reaches 4.7 μA. Computed transmission spectra of BN-p-3ZGNR (w = 4) under 0.0 and 2.0 V bias voltage are shown in Fig. 11(c) where a region of zero transmission with width of 1.12 eV under 0.0 V bias voltage is seen around the Fermi level, consistent with 1.14 eV band gap of BN-p-3ZGNR (w = 4). When the bias voltage is 2.0 V, the transmission peak appears around the Fermi level in the bias window [-1.0 V, 1.0 V]. Compared with the BN-3-Benzo-CMP sheet, BN-p-3ZGNR (w=4) possesses similar conductivity properties but a smaller band gap. So both materials are good candidates for applications in low-dimensional electronics.

4 Conclusions

In conclusion, we find that prototype 2D porous graphenes, namely, n-Benzo-CMPs (n=3, 4, 5) and BN-n-Benzo-CMPs (n=3, 4, 5), possess interesting structural, electronic and transport properties that are notably different from those of the graphene. These 2D materials are all semiconductors with direct band gaps ranging from 0.57 - 1.75 eV. They all have nanoscale pore size with diameter ranging from 3.68 - 12.93 Å. Their band gaps decrease with increasing the pore size. BN codoping tends to reduce their band gaps. 1D p-AGNRs and p-ZGNRs are also semiconductors. The band gaps of p-3AGNRs and p-3ZGNRs are slightly larger than that of the 3-Benzo-CMP sheet (~1.75 eV). With increasing the width of nanoribbons, the band gaps of p-3AGNRs and p-3ZGNRs decrease slightly. The band gaps of BN codoped p-GNRs are narrower than that of corresponding hydrocarbon p-GNRs. Also, the band gaps of BN codoped p-GNRs decrease with increasing the pore size, regardless of the chirality of nanoribbons. Computed electron transport properties suggest that the BN codoped derivatives exhibit better I–V_b characteristics. Especially, the BN-3-Benzo-CMP sheet and BN-p-3ZGNR (w = 4) are most promising candidate for applications in low-dimensional electronics. In closing, we note that Campbell *et.al* recently reported a hydroboration–oxidation procedure which can lead to undesired trimerization to BN-triphenylene (see Scheme 11 in Ref. 32). This experimental result suggests that the proposed BN-codoped structures in this study may be synthesized using a similar procedure in the laboratory.

Acknowledgements

ZDY is supported by scientific initial funding of National Ministry of Education for returned overseas. (grant No. [2014]1685) and the NSF of Heilongjiang Province of China (grant No. LC2015005). XCZ is supported by a grant from the US NSF through the Nebraska Materials Research Science and Engineering Center (MRSEC) (grant No. DMR-1420645). GLZ is supported by grants from the NSFC (51473042), the SF for leaders in academe of Harbin City of China (2013RFXXJ024), and the science foundation for backup leader of leading talent echelon in Heilongjiang province.

References

1 S. V. Morozov, K. S. Novoselov, M. I. Katsnelson, F. Schedin, L. A. Ponomarenko, D. Jiang, and A. K. Geim, *Phys. Rev. Lett*, 2006, **97**, 016801-016805.

2 M. Titov and C. W. J. Beenakker, *Phys. Rev. B*, 2006, **74**, 041401-041105.

3 H. B. Heersche, P. Jarillo-Herrero, J. B. Oostinga, L. M. K. Vandersypen and A. F. Morpurgo, *Nature*, 2007, **446**, 56-59.

4 S. Gilje, S. Han, M. Wang, K. L. Wang and R. B. Kaner, *Nano Lett*, 2007, **7**, 3394-3398.

5 H. C. Schniepp, J.-L. Li, M. J. McAllister, H. Sai, M. Herrera-Alonso, D. H. Adamson, R. K. Prud'homme, R. Car, D. A. Saville and I. A. Aksay, *J. Phys. Chem. B*, 2006, **110**, 8535-8539.

6 M. Bieri, M. Treier, J. Cai, K. At-Mansour, P. Ruffieux, O. Gröning, P. Gröning, M. Kastler, R. Rieger, X. Feng, K. Müllen and B. Fasel, *Chem. Commun.*, 2009, **45**, 6919–6921.

7 A. Du, Z. Zhu and S. C. Smith, *J. Am. Chem. Soc.*, 2010, **132**, 2876–2877.

8 M. Hatanaka, *Chem. Phys. Lett.*, 2010, **488**, 187–192.

9 Y. Li, Z. Zhou, P. Shen and Z. Chen, *Chem. Commun.*, 2010, **46**, 3672–3674.

10 Y. Ding, Y. Wang, S. Shi and W. Tang, *J. Phys. Chem. C*, 2011, **115**, 5334–5343.

11 G. Brunetto, P. A. S. Autreto, L. D. Machado, B. I. Santos, R. P. B. dos Santos and D. S. Galvão, *J. Phys. Chem. C,* 2012, **116**, 12810–12813.

12 E. Perim, R. Paupitz, P. A. S. Autreto and D. S. Galvao. *J. Phys. Chem. C.* 2014, **118**, 23670−23674.

13 M. Hatanaka, *J. Phys. Chem. C*, 2012, **116**, 20109–20120.

14 Y. Kou, Y. Xu, Z. Guo and D. Jiang, *Angew. Chem., Int. Ed.*, 2011, **50**, 8753–8757

15 Z. D.Yang, W.Wu and X. C. Zeng, *J. Mater. Chem. C*. 2014, **2**, 2902-2907.

16 X. Li, X. Wang, L. Zhang, S. Lee and H. Dai, *Science,* 2008, **319**, 1229-1232.

17 X. Wang, Y. Ouyang, X. Li, H. Wang, J. Guo and H. Dai, *Phys. Rev. Lett.* 2008, **100**, 206803-20806.

18 S. Ayissi, P. A. Charpentier, N. Farhangi, J. A. Wood, K. Palotás and W. A. Hofer, *J. Phys. Chem. C,* 2013, **117**, 25424−25432.

19 S. Okada and A. Oshiyama, *Phys. Rev. Lett*. 2001, **87**, 146803-146806.

20 B. Huang, Z. Li, Z. Liu,G. Zhou, S. Hao, J. Wu, B.-L. Gu and W. Duan, *J. Phys. Chem. C* 2008, **112**, 13442–13446.

21 D. Gunlycke, J. Li, J. W. Mintmire and C. T. White, *Nano Lett.* 2010, **10**, 3638–3642.

22 L. Zhu, J. Wang, T. Zhang, L. Ma, C. W. Lim, F. Ding and X. C. Zeng, *Nano Lett.* 2010, **10**, 494-498.

23 Y. Zhu, A. L. Higginbotham and J. M. Tour, *Chem. Mater.*, 2009, **21**, 5284–5291.

24 O. Hod, V. Barone, J. E. Peralta and G. E. Scuseria, *Nano Lett.* 2007, **7**, 2295-2299.

25 J. M. Soler, E. Artacho, J. D. Gale, A. Garc´ ıa, J. Junquera, P. Ordejón and D. Sánchez-Portal, *J. Phys.: Condens. Matter*, 2002, **14**, 2745–2779.

26 J. P. Perdew, K. Burke and M. Ernzerhof, *Phys. Rev. Lett.*, 1996, **77**, 3865–3868.

27 ATK, Version 13.8, atomistix a/s, **2013**, www.quantumwise.com.

28 M. Büttiker, Y. Imry, R. Landauer and S. Pinhas, *Phys. Rev. B: Condens. Matter Mater. Phys.*, 1985, **31**, 6207–6215.

29 X. Q. Shi, Z. X. Dai, G. H. Zhong, X. H. Zheng, Z. Zeng. *J. Phys. Chem. C* 2007**, 111***,* 10130.

30 X.-M. Wang, S.-S. Lu. *J. Phys. Chem. C* 2013, **117**, 19740.

31 W. Wu, W. Guo, X. C. Zeng, *Nanoscale*, 2013, **5**, 9264.

32 P. G. Campbell, A. J. V. Marwitz, S.-Y. Liu, *Angew. Chem. Int. Ed.* 2012, **51**, 6074

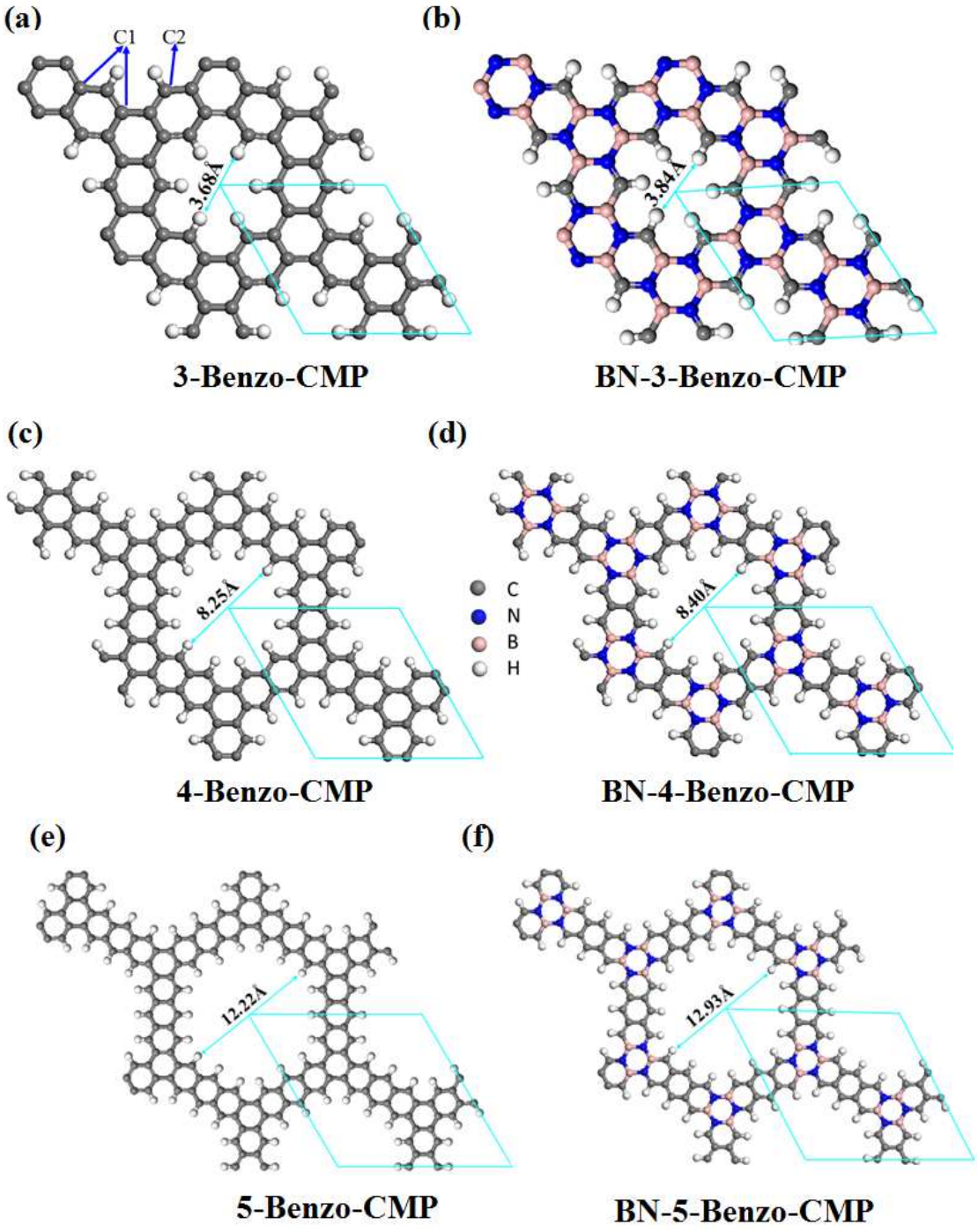

Fig. 1 Atomic structures of 2D (a) 3-Benzo-CMP, (b) BN-3-Benzo-CMP, (c) 4-Benzo-CMP, (d) BN-4-Benzo-CMP, (e) 5-Benzo-CMP and (f) BN-5-Benzo-CMP sheets in 2×2 supercell. The rhombus in (a) – (f) represents the unit cell. The gray, white, blue and pink balls denote C, H, N and B atoms, respectively.

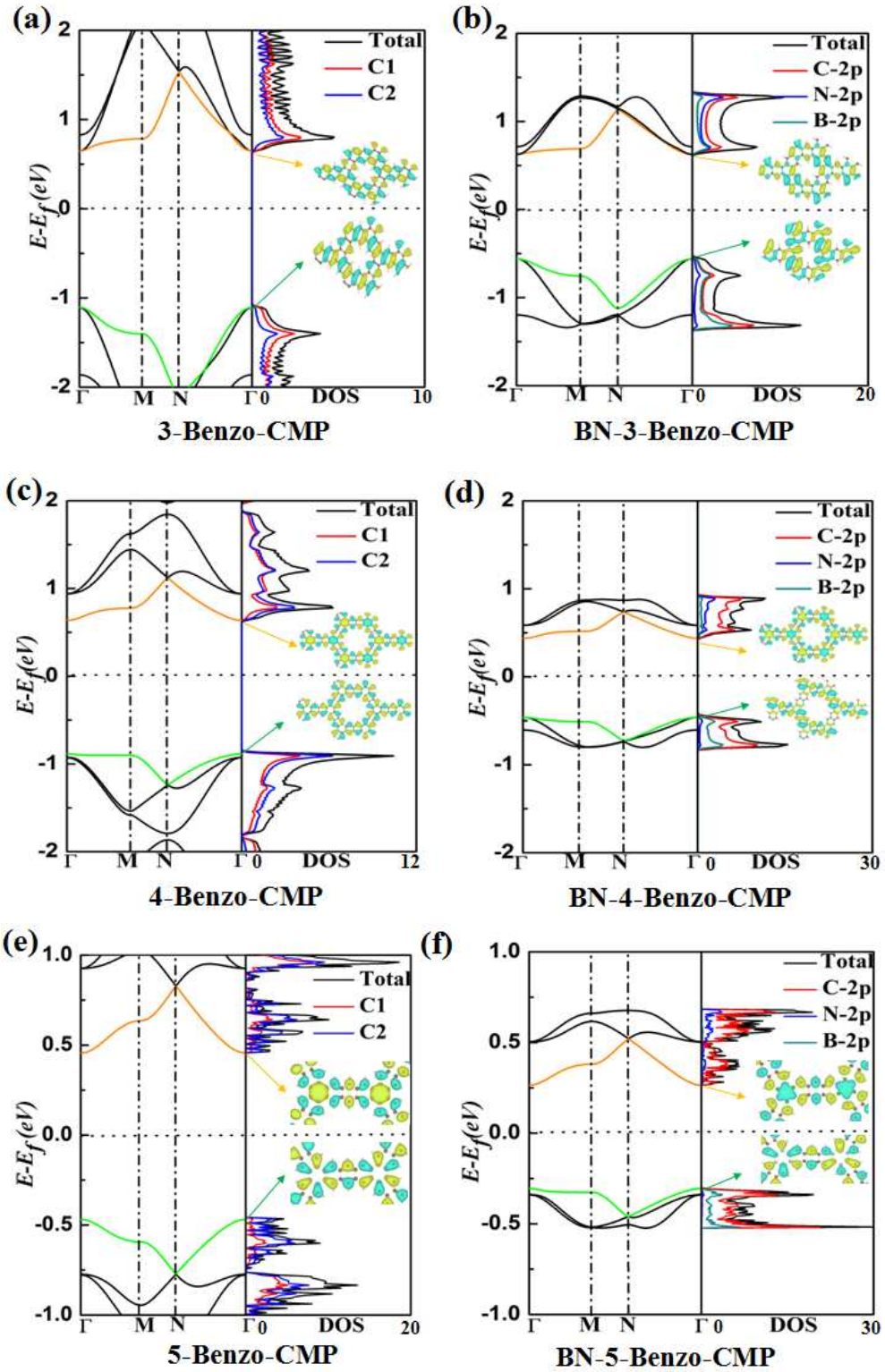

Fig. 2 Computed band structures (left panel) and total density of states and partial density of states (right panel) of *n*-Benzo-CMPs, and BN codoped derivatives in their primitive unit cell. The wave functions corresponding to the lowest conduction band and the highest valence band are plotted in the insets, where the isosurface corresponds to a value of 0.05 (e $Å^{-3}$).

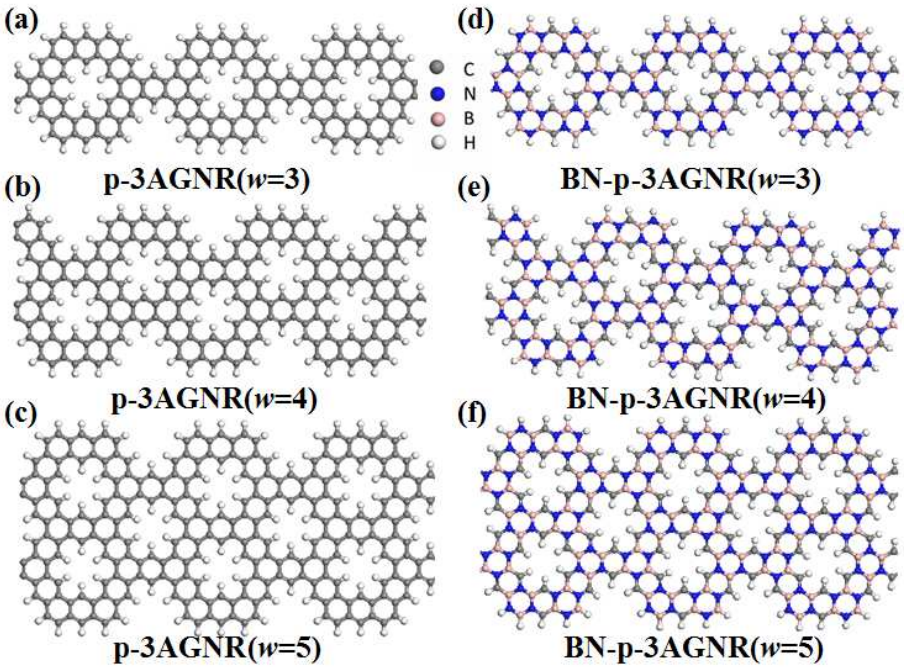

Fig. 3 Atomic structures of armchair porous graphene nanoribbons tailored from 3-Benzo-CMPs and BN-3-Benzo-CMPs in 1×1×3 supercell. (a) p-3AGNR (w = 3), (b) p-3AGNR (w = 4), (c) p-3AGNR (w = 5), (d) BN-p-3AGNR (w = 3), (e) BN-p-3AGNR (w = 4) and (f) BN-p-3AGNR (w = 5). The gray, white, blue and pink balls denote C, H, N, B, respectively, and w is the width factor.

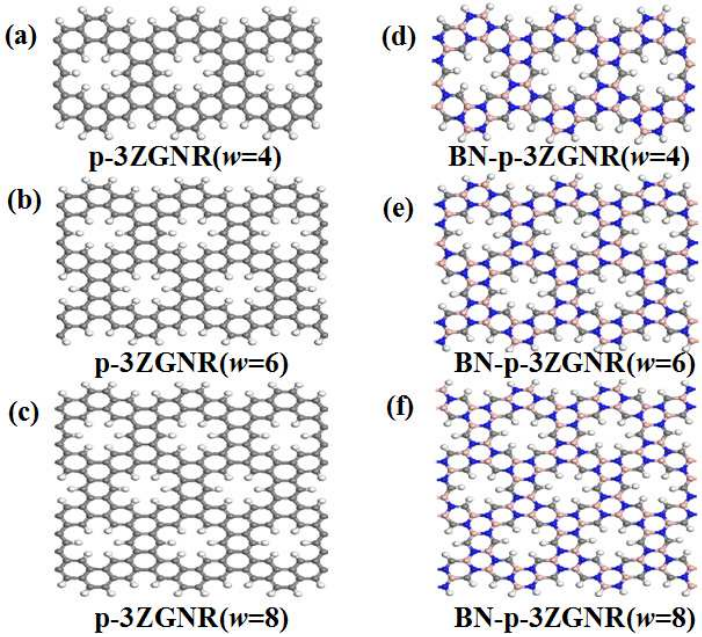

Fig. 4 Atomic structures of zigzag porous graphene nanoribbons tailored from 3-Benzo-CMPs and BN-3-Benzo-CMPs in 1×1×3 supercell. (a) p-3ZGNR (w = 4), (b) p-3ZGNR (w = 6), (c) p-3ZGNR (w = 8), (d) BN-p-3ZGNR (w = 4), (e) BN-p-3ZGNR (w = 6) and (f) BN-p-3ZGNR (w = 8)

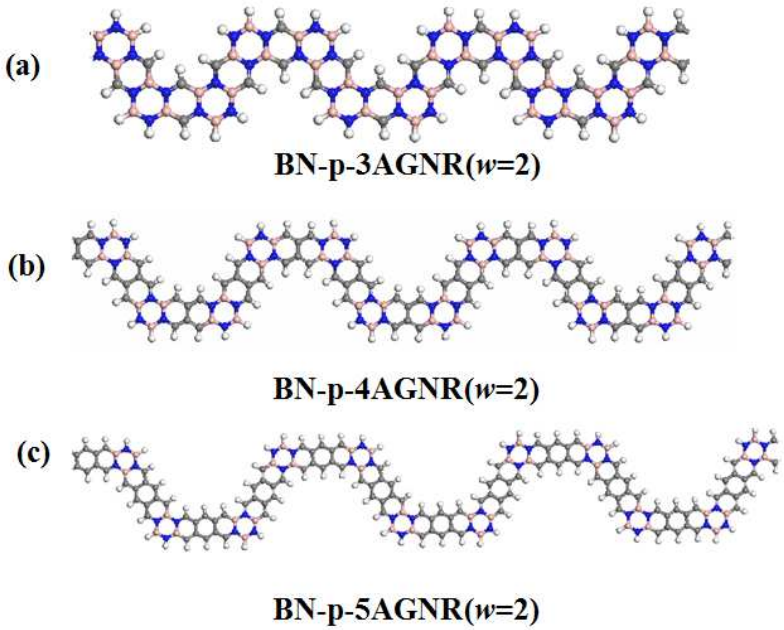

Fig. 5 Atomic structures of narrowest armchair porous graphene nanoribbons tailored from BN-3-Benzo-CMP, BN-4-Benzo-CMP and BN-5-Benzo-CMP with N_a=2

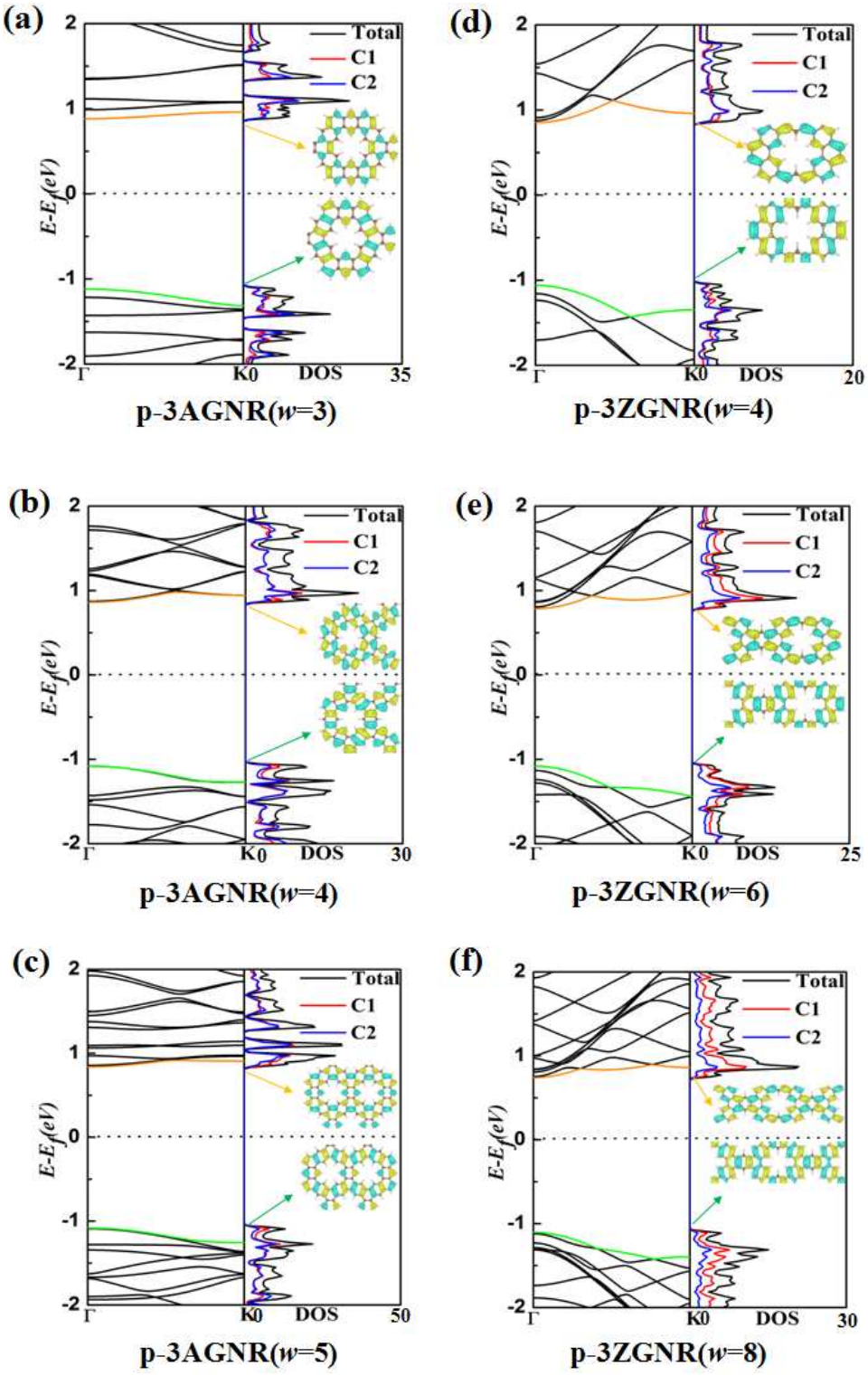

Fig. 6 Computed band structures (left panel) and total density of states and partial density of states (right panel) of 1D pure porous graphene nanoribbons of 3-Benzo-CMP: (a) p-3AGNR (w=3), (b) p-3AGNR (w=4), (c) p-3AGNR (w=5), (d) p-3ZGNR (w=4), (e) p-3ZGNR (w=6) and (f) p-3ZGNR (w=8). The wave functions corresponding to the lowest conduction band =and the highest valence band are plotted in the insets, where the isosurface corresponds to a value of 0.05 (e Å^{-3}).

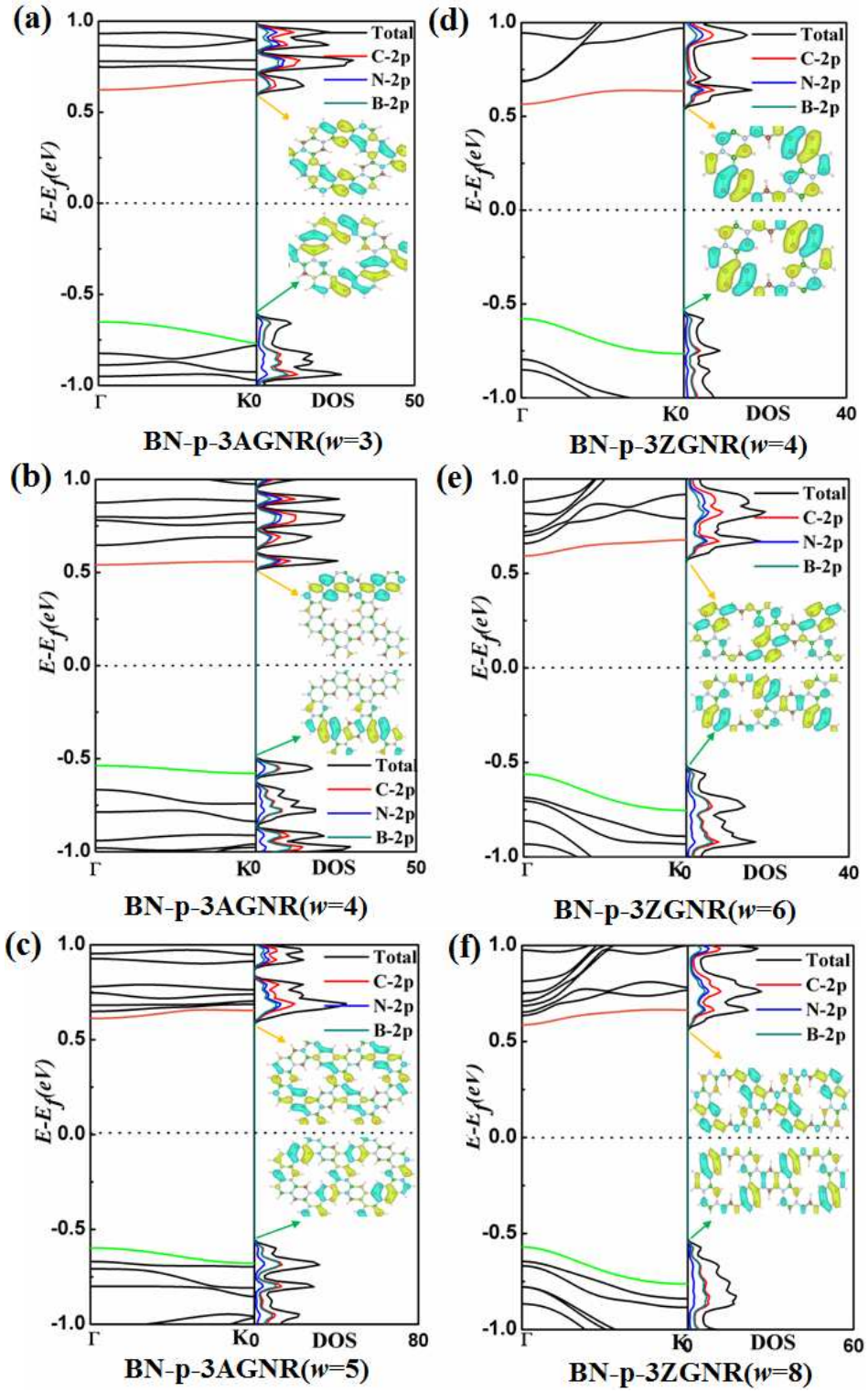

Fig. 7 Computed band structures (left panel) and total density of states and partial density of states (right panel) of 1D BN-doped porous graphene nanoribbons of BN-3-Benzo-CMP: (a) BN-p-3AGNR (w = 3), (b) BN-p-3AGNR (w = 4), (c) BN-p-3AGNR (w = 5), (d) BN-p-3ZGNR (w = 4), (e) BN-p-3ZGNR (w = 6) and (f) BN-p-3ZGNR (w = 8).

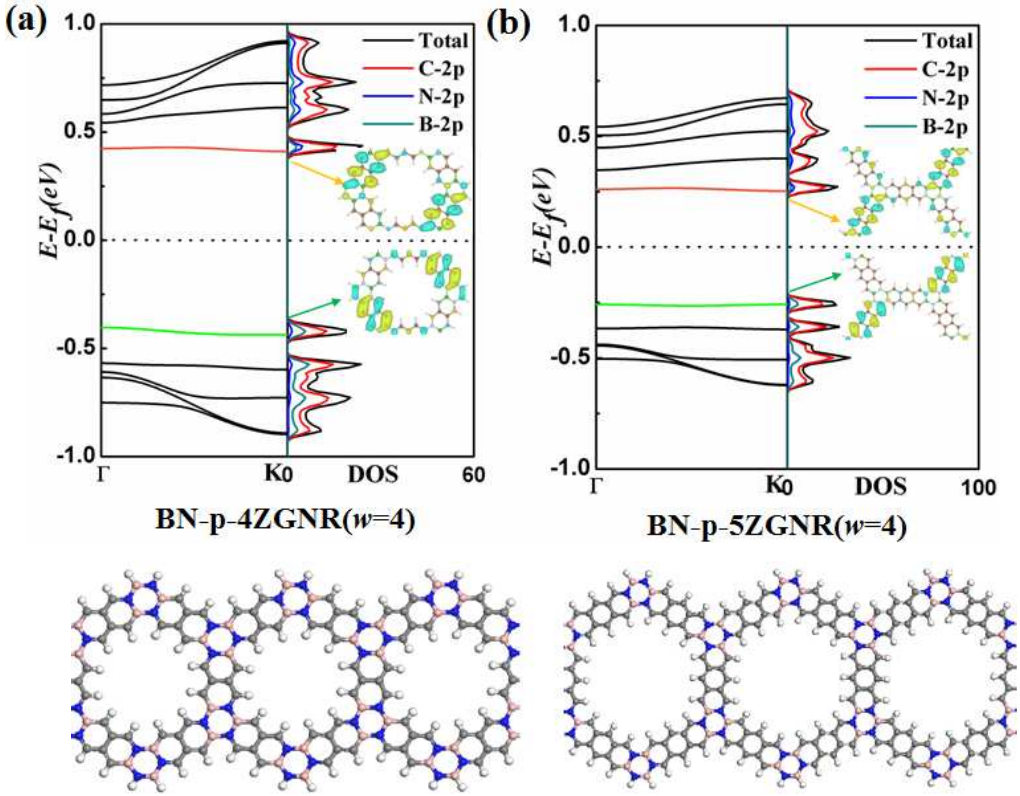

Fig. 8 Computed band structures (left panel) and total density of states and partial density of states (right panel) of BN codoped zigzag porous graphene nanoribbons tailored from BN-4-Benzo-CMP and BN-5-Benzo-CMP:(a) BN-p-4ZGNR (w = 4) (structure shown in lower panel) and (c) BN-p-5ZGNR (w = 4) (structure shown in lower panel).

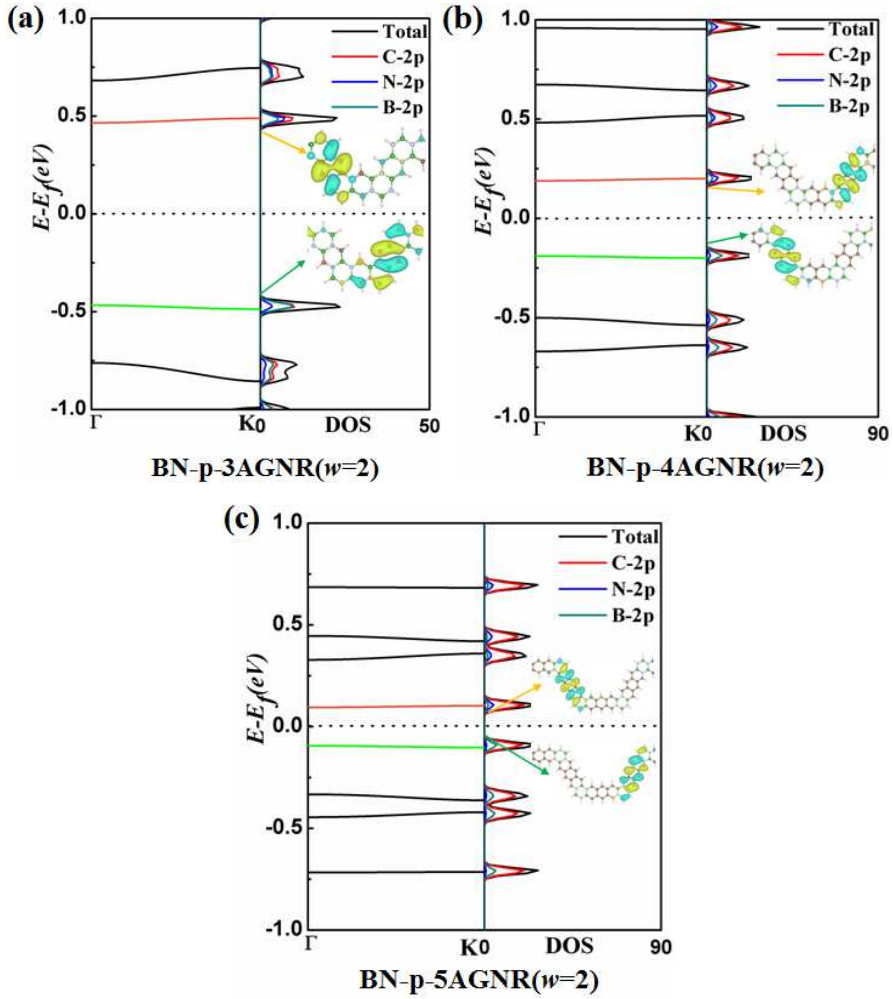

Fig. 9 Computed band structures (left panel) and total density of states and partial density of states (right panel) of BN codoped armchair porous graphene nanoribbons. (a) BN-p-3AGNR (w = 2), (b) BN-p-4AGNR (w = 2) and (c) BN-p-5AGNR (w = 2).

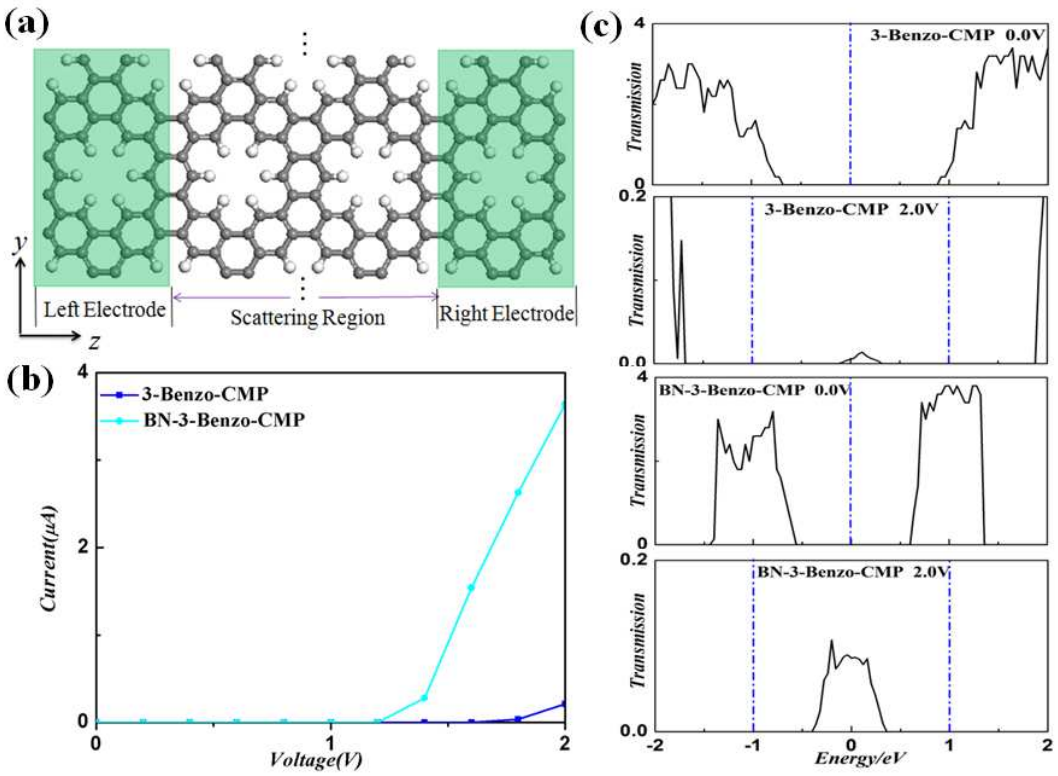

Fig. 10 (a) Schematic view of the two-probe system of 3-Benzo-CMP; (b) variation of current as a function of the bias voltage (I–V_b curves) of 3-Benzo-CMP and BN-3-Benzo-CMP; (c) computed transmission spectra under 0.0 and 2.0 bias voltage.

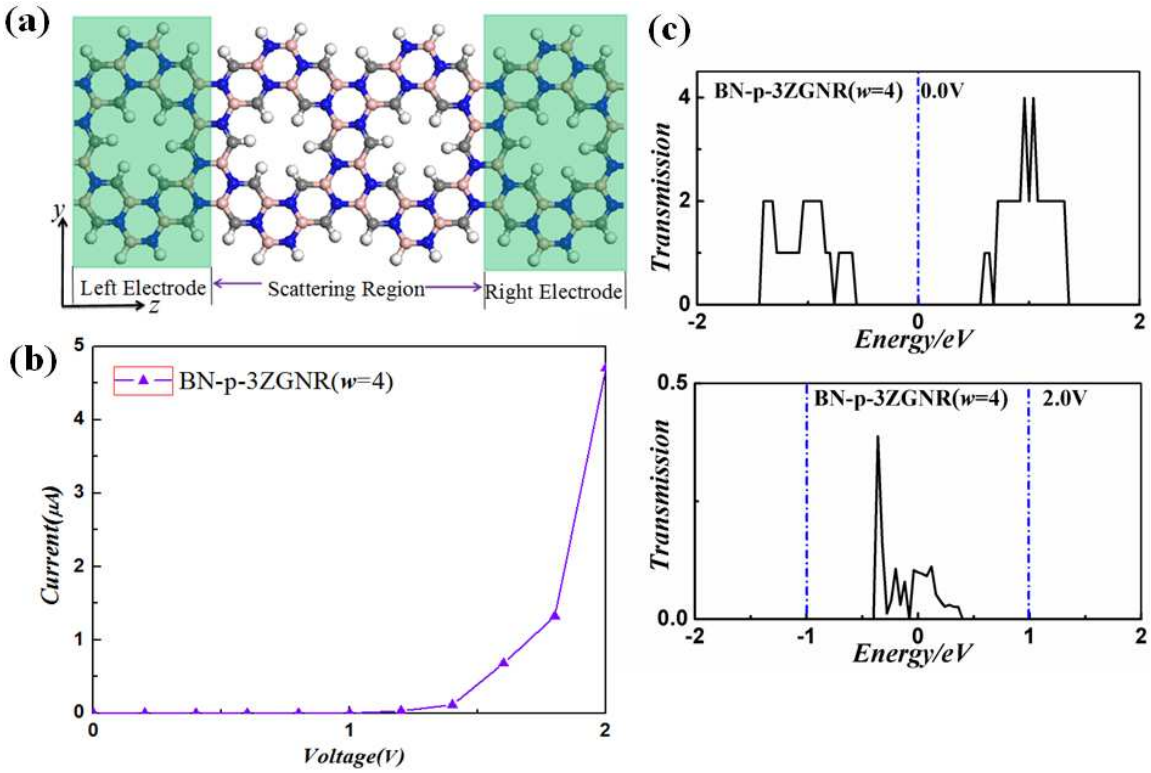

Fig. 11 Schematic view of the two-probe system of BN-p-3ZGNR (w =4); (b) variation of current as a function of the bias voltage (I–V_b curve) of BN-p-3ZGNR (w = 4); (c) computed transmission spectra of BN-p-3ZGNR (w = 4) under 0.0 and 2.0 bias voltage.

Table 1 Optimized lattice parameters (b=c), and computed band gaps of 2D n-Benzo-CMPs (n=3, 4, 5) sheets and their BN-codoped derivatives

n-Benzo-CMPs	Lattice parameters(Å)	Band gaps (eV)	BN-n-Benzo-CMPs	Lattice parameters(Å)	Band gaps (eV)
n=3	8.64	1.75	n=3	8.83	1.19
n=4	12.90	1.52	n=4	13.08	0.90
n=5	17.27	0.92	n=5	17.36	0.57

Table 2 Optimized lattice parameters, and computed band gaps of all 1D armchair- and zigzag-edged p-GNRs

type	p-GNRs	Lattice parameters(Å)	Band gaps (eV)
Armchair	p-3AGNR (w=3)	14.97	2.00
	p-3AGNR (w=4)	14.97	1.94
	p-3AGNR (w=5)	14.97	1.92
	BN-p-3AGNR (w=3)	15.30	1.27
	BN-p-3AGNR (w=4)	15.30	1.08
	BN-p-3AGNR (w=5)	15.30	1.21
	BN-p-3AGNR (w=2)	15.29	0.93
	BN-p-4AGNR (w=2)	22.67	0.38
	BN-p-5AGNR (w=2)	30.06	0.19
Zigzag	p-3ZGNR (w=4)	8.64	1.91
	p-3ZGNR (w=6)	8.64	1.87
	p-3ZGNR (w=8)	8.64	1.84
	BN-p-3ZGNR (w=4)	8.84	1.14
	BN-p-3ZGNR (w=6)	8.84	1.15
	BN-p-3ZGNR (w=8)	8.84	1.16
	BN-p-4ZGNR (w=4)	13.08	0.83
	BN-p-5ZGNR (w=4)	17.37	0.52

Graphic Abstract